PHYSICAL REVIEW E **77**, 010401(R) (2008)

Monte Carlo simulations of in-plane stacking disorder in hard-sphere crystals

P. S. Miedema, V. W. A. de Villeneuve, and A. V. Petukhov
Van 't Hoff Laboratory for Physical and Colloid Chemistry, Department of Chemistry, Faculty of Science, Utrecht University, Padualaan 8, 3584 CH Utrecht, The Netherlands

(Received 10 August 2007; published 2 January 2008)

On-lattice Monte Carlo simulations of colloidal random-stacking hard-sphere colloidal crystals are presented. The model yields close-packed crystals with random-stacking hexagonal structure. We find a significant amount of in-plane stacking disorder, which slowly anneals in the course of the simulation. The in-plane stacking disorder leads to lateral broadening of the stacking-disorder-induced Bragg rods. It is found that not only the scattering intensity, but also the width is modulated along the Bragg rods.

DOI: 10.1103/PhysRevE.77.010401 PACS number(s): 82.70.Dd, 61.05.cc, 61.72.Nn

Hard spheres are the simplest particles which can undergo a phase transition: due to a gain in excluded-volume entropy, they spontaneously form close-packed crystals at sufficiently high concentrations. The most efficient packing of spheres can be achieved by arranging them into stacked hexagonal-close-packed planes [1]. Stacking sequences of *ABCABC* and *ABABAB* types lead to face-centered-cubic (fcc) and hexagonal-close-packed (hcp) structures, respectively. Although the fcc structure is somewhat more favored over hcp structure [2–4], the entropy difference between these two structures is very small, less than $10^{-3}k_BT$ per particle, where kBT is the thermal energy. As a consequence, random hexagonal-close-packed (RHCP) structures are often encountered in experimental systems [5–7].

Hard spheres are experimentally accessible by resorting to colloidal particles [8,9]. These systems are sufficiently slow in time to study the dynamics of the system and sufficiently large to be studied in real space by, most notoriously, confocal microscopy [10]. Such studies have augmented the understanding of crucial aspects of hard-sphere crystallization [11,12] and have adequately characterized various types of disorder [5,13] as well as defect dynamics [14,15]. The structure of colloidal crystals can also be studied using diffraction techniques using light [6,16,17], neutrons [18,19], or x-rays [19–22]. In the diffraction domain the stacking disorder in RHCP crystals smears out some of the diffraction peaks into the so-called Bragg scattering rods oriented perpendicular to the hexagonal-close-packed planes of the crystal [19,20,23]. At the same time, the reflections, where the fcc and hcp reciprocal lattice coincide, do not depend on the stacking sequence and remain sharp in all three directions. In this work they are referred to as Bragg spots. The recent advance of microradian x-ray diffraction [21,22] allows a determination of the intrinsic width of the diffraction peaks. In particular, it was recently discovered that the Bragg rods are also slightly broadened in the direction parallel to the hexagonal planes [21]. This observation suggests that the crystal planes consist of islands with different lateral positions (usually denoted *A*, *B*, and *C*). As a result, the stacking sequence varies not only between the planes, but also along the planes. Such island structure in hard-sphere colloidal crystals was indeed found by laser confocal microscopy [5].

The existence of in-plane stacking disorder in RHCP crystals can be understood within a simple nucleation-and-growth model: if every new crystal plane nucleates at multiple locations, in-plane stacking disorder is unavoidable because the lateral position at every nucleation center is chosen at random. In our previous publication results of a theoretical investigation within a layer-by-layer nucleation-and-growth model, applied to small crystallites, have been presented [24]. In this work we simulate the in-plane stacking disorder using a distinctly different model without any nucleation barrier. Instead, the formation and the growth of lateral islands are driven by the need for a more effective packing of the particles. Therefore, in this model the evolution of islands can be studied while in our previous approach only static structures were obtained. Moreover, the current model distinguishes the coordinates of the particles at different stacking positions. The obtained real-space structures are used to study the effect of the in-plane stacking disorder on the diffraction patterns.

The random-stacking crystal structures are generated using on-lattice Monte Carlo (MC) simulations. The particles can occupy nodes of a simple hexagonal lattice of *A*, *B*, and *C* positions. Within the hexagonal planes the distance between the neigboring positions (along the *x* axis) is equal to $\sigma/\sqrt{3}$, where σ is the particle diameter. Thus, if a particle occupies a certain lattice position at, e.g., an *A* node, six nearest positions (three of *B* and three of *C* type) are excluded for other particles. The distance between the hexagonal planes is taken as $d_z=\sigma\sqrt{2/3}$ so that two sites exactly above each other (i.e., with the same lateral position) cannot be occupied simultaneously. The size of the simulation box is determined by the number of *A*, *B*, and *C* positions along a row of nodes in the *x* direction, N_x, the number of such rows in the *y* direction, N_y, and the number of hexagonal planes, N_z. The maximum number of particles, which can fit into the simulation box (for a perfect close-packed structure), is equal to $(N_x\times N_y\times N_z)/3$. Periodic boundary conditions are used. In this paper we present results for the box size of $(N_x\times N_y\times N_z)=(90\times 90\times 30)$.

An elementary MC attempt consists of choosing one of the lattice positions at random. If this position is unoccupied, a particle insertion attempt is made. If it is occupied, a particle displacement to one of its six nearest-neighbor positions within the same plane is attempted. An attempt is accepted if no overlap with other particles is created. One MC step was defined as $N_x\times N_y\times N_z$ elementary attempts—i.e., one attempt per lattice site on average. The results were averaged

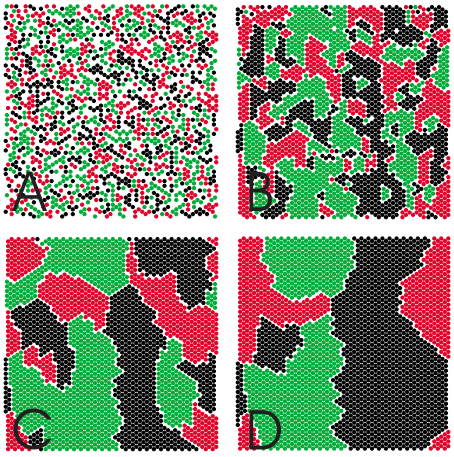

FIG. 1. (Color online) Characteristic development of the island structure within a close-packed plane after 1 MC step (A), 32 MC steps (B), 256 MC steps (C), and 1024 MC steps (D). Particles at *A*, *B*, and *C* positions are denoted by different colors.

over N_{av} random realizations of the structure (starting from an empty lattice).

In Fig. 1 the typical configurations within one of the planes are shown for different MC times, where different lateral positions are denoted by different colors. After one MC step the structure is rather disordered and no clear islands can be seen. Upon subsequent MC simulations the particles start to form islands with identical lateral positions [see panel (B) after 32 MC steps]. The islands are slowly growing in time and, after about 1024 MC steps, the islands become comparable to the simulation box size in the *x* and *y* directions and artifacts related to the finite size of the simulation box can come into play.

After every MC step a number of parameters such as the average island dimension and the fraction of fcc stacked particles α are calculated. The island dimension $D_{\mathrm{isl}}=\sqrt{N_{\mathrm{isl}}}$ is defined as the square root of the average amount N_{isl} of particles per island with the same lateral position. In Fig. 2(A) the development of D_{isl} in the course of the MC simulation is presented. The later stages of this MC simulation could be compared to confocal microscopy studies of the evolution of a crystal structure formed through epitaxial growth such as in Ref. [25]. The template should be such that the lateral positions *A*, *B*, and *C* are all available for growth.

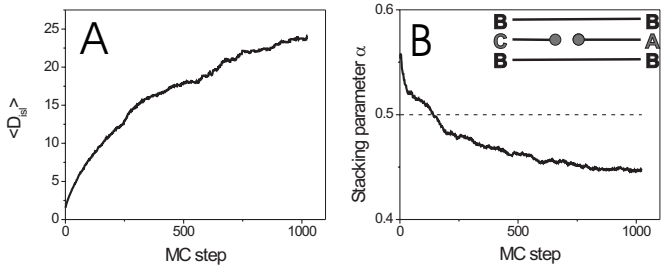

FIG. 2. Development of the average island dimension (A) and the stacking parameter α (B) in the course of the MC simulations. The inset in (B) sketches closure of a single line defect. The results are averaged over $N_{\mathrm{av}}=100$ realizations. The dashed line represents $\alpha=0.5$, which is perfect RHCP.

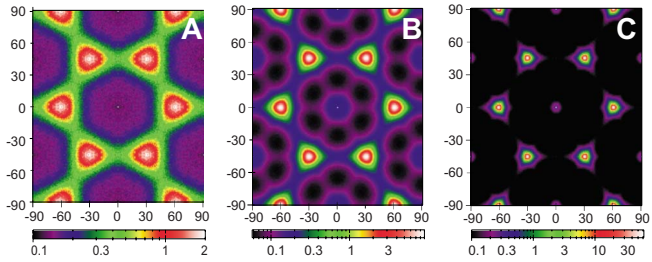

FIG. 3. (Color online) Structure factor pattern in the x,y plane at $q_z=0$ after 8 MC steps [(A), $N_{\mathrm{av}}=100$], after 64 MC steps [(B), $N_{\mathrm{av}}=700$], and after 512 MC steps [(C) $N_{\mathrm{av}}=300$].

The fraction of fcc stacked particles α was calculated using the orientational correlation method (ψ_3), elaborately described in Ref. [5]. As shown in Fig. 2(B), α tends to slightly reduce during the simulation. An explanation might be that the closure of line defects requires creation of hcp environments. For example, as illustrated in the inset of Fig. 2(B), in the case of a single line defect the islands on both sides of a line defect have a hcp environment. Nevertheless, the value of α does not drop much and remains close to a value of $\alpha=0.5$.

Utilizing the obtained configurations in real space the structure factor $S(\vec{q})$ is obtained using

$$S(\vec{q})=\left\langle \frac{1}{N}\left|\sum_i \exp[iq_x x_i+iq_y y_i+iq_z z_i]\right|^2\right\rangle, \qquad (1)$$

where x_i, y_i, and z_i are the Cartesian coordinates of the *i*th particle and *N* is the number of particles. The angular brackets indicate averaging over different realizations of the structure. The calculations are performed on a discrete grid of wave vector $\vec{q}$ values with the sampling rate, which is determined in every Cartesian direction α by the corresponding size of the simulation box L_α

$$q_\alpha=\frac{2\pi n_\alpha}{L_\alpha}, \qquad (2)$$

where n_α is an integer. The structure factor $S(\vec{q})$ is calculated for the values of q_α running from 0 to the Nyquist critical frequency, which is related to the sampling rate in the real space. In the *x* direction the Nyquist critical frequency is reached at $n_x=N_x$ while in the *y* and *z* directions it corresponds to $n_y=N_y/2$ and $n_z=N_z/2$.

Examples of two-dimensional structure factor patterns $S(q_x,q_y,q_z=0)$ are presented in Fig. 3 for three different MC times. Here the beam is assumed to be orthogonal to the hexagonal crystal planes (thus, $q_z=0$). The patterns are reconstructed from the irreducible part of the Brillioun zone using the pattern symmetry. Two types of peaks show up. The first type originate from the stacking-independent Bragg spots at $(n_x,n_y)=(0,0)$, $(N_x,Ny/2)$, $(0,Ny)$, etc. Since all occupied lattice positions contribute with the same phase to the stucture factor at these values of *q*, these peaks are very sharp (only one pixel wide). The Bragg spots are surrounded by weak "halos" originating from the fluctuation of the den-

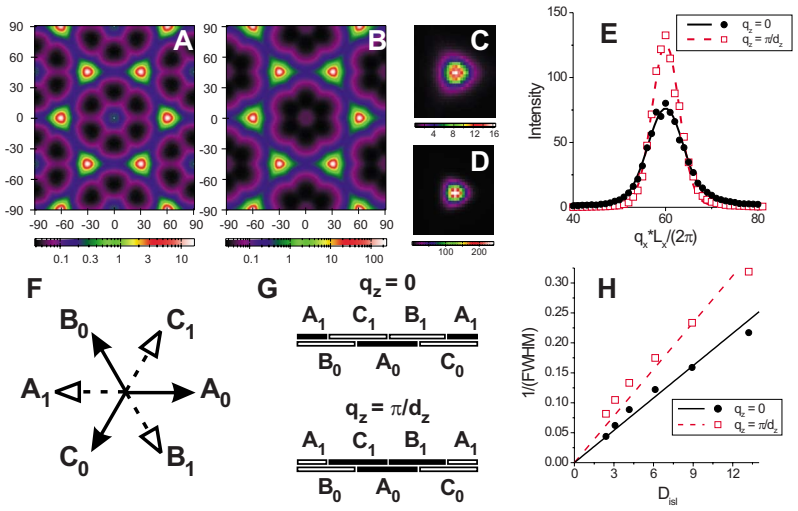

FIG. 4. (Color online) Structure factor patterns within the x,y planes at $q_z=0$ (A) and $q_z=\pi/d_z$ (B) after 128 MC steps (logarithmic intensity scale). $N_{\mathrm{av}}=700$. Panels (C) and (D) present close-ups (linear intensity scale) of the Bragg rod cross sections at $(n_x,n_y)=(60,0)$ from the patterns shown in (A) and (B), respectively. Panel (E) presents profiles of the structure factor across the Bragg rod at $q_z=0$ (solid circles) and $q_z=\pi/d_z$ (open squares). The symbols are the simulation results and the lines are the Gaussian fits of the line profiles. Panel (F) illustrates the phases of the contributions of different islands in two adjacent crystal planes at $q_z=\pi/d_z$. Panel (G) sketches a possible island structure in two subsequent crystal planes (side view). Islands, which interfere constructively with island A_0, are denoted by solid bars, while open bars correspond to islands yielding destructive interference. The top and bottom sketches correspond to $q_z=0$ and $q_z=\pi/d_z$, respectively. Panel (H) displays a plot of the inverse width of the Bragg rod at $q_z=0$ and $q_z=\pi/d_z$ as a function of the island dimension determined in real space. The symbols display results of the data analysis while the lines are meant to guide the eye.

sity of occupied states on a scale larger than the lattice period. The second type of reflections [e.g., at $(n_x,n_y)=(2N_x/3,0)$, $(N_x/3,Ny/2)$, etc.] are much broader, and they originate from an intersection of the Bragg rods by the Ewald sphere. These peaks clearly sharpen with MC time (note the variation of the intensity scale in the patterns). In addition, one can also see some anisotropy of the scattering background around the peaks. Since no thermal motion of the colloidal particles is included in the model, the scattering background originates from the boundaries between the islands. Since the orientation of the boundaries is correlated with the underlying hexagonal symmetry, their contribution to the scattering field in between the peaks displays significant anisotropy.

So far, the results have been presented at $q_z=0$. To explore the third dimension in reciprocal space, a cross section of the reciprocal space by an x,y plane at $q_z=\pi/d_z$ was calculated. The results at $q_z=0$ and $q_z=\pi/d_z$ are compared with each other in Figs. 4(A) and 4(B). Note that in an experiment one can only measure a cut through the three-dimensional (3D) reciprocal space by the so-called Ewald sphere that goes through the origin of the reciprocal space $\vec{q}=0$. Thus, a pattern such as shown in Fig. 4(B) cannot be measured directly. However, the full 3D reciprocal space can be reconstructed by measuring the diffraction pattern with different orientations of a colloidal crystal and therefore the pattern of Fig. 4(B) can in principle also be calculated from the experimental data.

At $q_z=\pi/d_z$ the x,y plane lacks the stacking-independent Bragg spots and the δ-function-like reflections disappear. According to Wilson's theory [23], the structure factor along the Bragg scattering rod displays a maximum at this value of q_z. For example, for a random-stacking crystal with $\alpha=0.5$, it follows that $S_{\mathrm{rod}}(q_z=\pi/d_z)=9S_{\mathrm{rod}}(q_z=0)$. This striking increase in the structure factor is observed in the present results as well (note the change in the intensity scale bar). A closer look at the patterns reveals a difference in the peak widths as well. This difference is more clear in panels (C) and (D) of Fig. 4, which present close-ups of the reflections using a linear intensity scale. To quantify the peak widths, the profiles of the structure factor were fitted by a Gaussian function along x, as shown in panel (E). The full width at half maximum (FWHM) of the obtained fits was used as a measure of the peak width, which was found to vary by more than 30% and should therefore be observable experimentally.

The variation of the width of the Bragg rod along q_z can be understood as an effect of the correlations in the island structure of adjacent layers. As illustrated in panel (F), a change in the lateral position of the particles within the same crystal plane changes the phase of their contribution to scattering by ±120°. As a result, the contributions of islands A_0, B_0, and C_0 interfere destructively for both $q_z=0$ and $q_z=\pi/d_z$. The contributions of particles in a adjacent plane, however, depend on the value of q_z. At $q_z=0$ the phases do not depend on the z coordinate of the crystal plane while at $q_z=\pi/d_z$ there is an additional phase difference of 180° between their contributions. As a result, the A_0 island in the bottom plane interferes destructively with the contribution of the A_1 islands in the top crystal plane while its interference with B_1 and C_1 islands is rather constructive. This effect is illustrated schematically in panel (G) using an example of possible island structure in two adjacent planes. Due to the mutual exclusion rule (no A on A is possible), an A_1 island in the top plane cannot begin before the A_0 island in the bottom

plane ends. The lateral dimension of an area that contributes constructively with the A_0 island to the Bragg rod at $q_z=\pi/d_z$ is therefore somewhat larger than the corresponding area at $q_z=0$. This variation of the lateral extent of the constructive interference between two layers leads to the difference of the widths of the Bragg rod at these two values of q_z.

Finally, the relation between the width of the Bragg rod and the island dimension [see Fig. 2(A)] is illustrated in Fig. 4(H). One can see that the peak width is approximately inversely proportional to the island dimension as determined by analyzing the real-space data. The slight deviation from the inverse proportionality might be related to the fact that the island shape varies in the course of the Monte Carlo simulation. At earlier stages the islands show somewhat more open shapes including relatively long branches and inclusions of other islands inside them [see Fig. 1(B)]. Later the islands tend to display more compact shapes [see Fig. 1(C)]. At all stages of the simulation one can see a remarkable difference in the width of the Bragg rod at $q_z=0$ and $q_z=\pi/d_z$.

In experimental systems the Bragg rods can be broadened due to various effects such as mosaicity or second-type disorder (lattice deformations) [13]. Despite these effects, broadening of the rods due to the island structure can be experimentally observed. So far, it was detected only at $q_z=0$ [21]. To confirm the prediction of the present calculations, we are planning to study the width of the Bragg rods with microradian x-ray diffraction at other crystal orientations. Diffraction of visible light can also be used to observe the predicted width modulation if one uses sufficiently large single colloidal crystals.

In summary, our Monte Carlo simulations generate various realisations of the colloidal crystals with random hexagonal-close-packed structure. The model yields strong in-plane stacking disorder, which slowly anneals during the simulation. The obtained structures are used to calculate scattering patterns. We have observed a significant broadening of the stacking-disorder-induced Bragg rods. Moreover, the interplane positional correlations lead not only to the modulation of the structure factor along the Bragg rod; its width periodically varies as well.

We would like to thank Jan Groenewold and Anke Leferink op Reinink for fruitful discussions. Professor H.N.W. Lekkerkerker is gratefully acknowledged for his support. The work of V.W.A.d.V. is part of the research program of the "Stichting voor Fundamenteel Onderzoek der Materie" (FOM), which is financially supported by the "Nederlandse Organisatie voor Wetenschappelijk Onderzoek" (NWO). Support of V.W.A.d.V. by the DFG through the SFB TR6 is acknowledged.

[1] N. J. A. Sloane, Nature (London) **395**, 435 (1998).
[2] P. G. Bolhuis, D. Frenkel, S. C. Mau, and D. A. Huse, Nature (London) **388**, 235 (1997).
[3] A. D. Bruce, N. B. Wilding, and G. J. Ackland, Phys. Rev. Lett. **79**, 3002 (1997).
[4] S. C. Mau and D. A. Huse, Phys. Rev. E **59**, 4396 (1999).
[5] J. M. Meijer, V. W. A. de Villeneuve, and A. V. Petukhov, Langmuir **23**, 3554 (2007).
[6] W. K. Kegel and J. K. G. Dhont, J. Chem. Phys. **112**, 3431 (2000).
[7] M. S. Elliot, B. T. F. Bristol, and W. C. K. Poon, Physica A **235**, 216 (1997).
[8] R. P. A. Dullens, D. G. A. L. Aarts, and W. K. Kegel, Proc. Natl. Acad. Sci. U.S.A. **103**, 529 (2006).
[9] P. N. Pusey and W. van Megen, Nature (London) **320**, 340 (1986).
[10] V. Prasad, D. Semwogerere, and E. R. Weeks, J. Phys.: Condens. Matter **19**, 113102 (2007).
[11] U. Gasser, E. R. Weeks, A. Schofield, P. N. Pusey, and D. A. Weitz, Science **292**, 258 (2001).
[12] R. P. A. Dullens, D. G. A. L. Aarts, and W. K. Kegel, Phys. Rev. Lett. **97**, 228301 (2006).
[13] R. P. A. Dullens and A. V. Petukhov, Europhys. Lett. **77**, 58003 (2007).
[14] R. P. A. Dullens and W. K. Kegel, Phys. Rev. E **71**, 011405 (2005).
[15] P. Schall, I. Cohen, D. A. Weitz, and F. Spaepen, Science **305**, 1944 (2004).
[16] C. Dux and H. Versmold, Phys. Rev. Lett. **78**, 1811 (1997).
[17] V. C. Martelozzo, A. B. Schofield, W. C. K. Poon, and P. N. Pusey, Phys. Rev. E **66**, 021408 (2002).
[18] S. M. Clarke, A. R. Renie, and R. H. Otterwill, Langmuir **13**, 1964 (1997).
[19] H. Versmold, S. Musa, and A. Bierbaum, J. Chem. Phys. **116**, 2658 (2002).
[20] I. P. Dolbnya, A. V. Petukhov, D. G. A. L. Aarts, G. J. Vroege, and H. N. W. Lekkerkerker, Europhys. Lett. **72**, 962 (2005).
[21] A. V. Petukhov, J. H. J. Thijssen, D. C. 't Hart, A. Imhof, A. van Blaaderen, I. P. Dolbnya, A. Snigirev, A. Moussaid, and I. Snigireva, J. Appl. Crystallogr. **39**, 137 (2006).
[22] J. H. J. Thijssen, A. V. Petukhov, D. C. 't Hart, A. Imhof, C. H. M. van der Werf, E. I. Schropp, and A. van Blaaderen, Adv. Mater. (Weinheim, Ger.) **18**, 1662 (2006).
[23] A. J. C. Wilson, *X-Ray Optics* (Methuen, London, 1949).
[24] V. W. A. de Villeneuve, P. S. Miedema, J. M. Meijer, and A. V. Petukhov, Europhys. Lett. **79**, 56001 (2007).
[25] J. P. Hoogenboom, A. K. van Langen-Suurling, J. Romijn, and A. van Blaaderen, Phys. Rev. E **69**, 051602 (2004).